

# High performance, single etch step MMI design on SOI

Robert Halir, Íñigo Molina Fernández, Alejandro Ortega Moñux, Juan Gonzalo Wangüemert Pérez, (1)  
Dan-Xia Xu, Pavel Cheben and Siegfried Janz (2)

1) Departamento de Ingeniería de Comunicaciones, Universidad de Málaga, Spain, robert.halir@ic.uma.es

2) Institute for Microstructural Sciences, National Research Council, Canada, pavel.cheben@nrc-cnrc.gc.ca

**Abstract:** We present a design criterion for high performance Silicon-on-Insulator (SOI) Multi-Mode Interference couplers (MMIs) based on single etch step rib waveguides. We design a shallowly etched  $2 \times 2$  coupler with an excess loss of only 0.1dB and an imbalance of less than 0.02dB for both TE and TM polarizations.

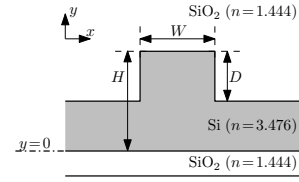
## 1 Introduction

Multimode interference couplers (MMIs) [1] are commonly used in photonic integrated circuits (PICs) as power splitters, combiners and directional couplers, because of their ease of fabrication, high bandwidth, compactness and polarization insensitivity [2].

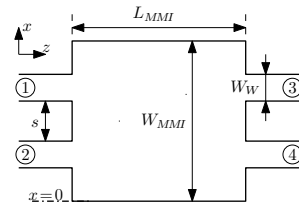
Silicon on Insulator (SOI) in turn has attracted a lot of attention in the last years since it offers a very high index contrast ( $\Delta n \approx 2$ ) allowing for high light confinement and thus very compact devices. Other advantages of the SOI platform are its potential compatibility with CMOS technology [3], and the availability of high quality wafers, since they have been used for years in the CMOS industry.

The most commonly used waveguides on SOI are rib waveguides (see fig. 1(a)), as they can have a large cross section while still being practically single-moded [4][5]. The design of rib waveguide based MMIs on SOIs still poses some challenges: for the waveguide to be potentially single-moded, it has to be shallowly etched ( $D \leq \frac{H}{2}$ ), but with this type of etching it seems to be difficult to achieve low excess loss and imbalance. For instance, even for relatively simple MMI configuration such as  $1 \times 2$  splitter, a minimum imbalance of 0.28dB has been reported for a fabricated device in [6]. Simulations of a  $1 \times 4$  splitter in [7] show an imbalance of 0.37dB and excess losses of 1.37dB. These relatively high losses are believed to be caused by imperfect imaging due to the shallow etching, which is why the authors of [7] propose a two etch step design, where both the access waveguides and the multimode section are deeply etched. While simulations show that such a design yields a nearly perfect imaging and very low losses, the fact that it requires two etching steps makes it more difficult and expensive to fabricate these devices. In fact, a fabricated MMI where only the multimode section is deeply etched is reported in [8], where a specific fabrication process is developed.

In this communication we show that by adequately designing the shallowly etched access waveguides it is possible to achieve high performance MMIs with a single etch step fabrication process. Our simulations of a  $2 \times 2$  coupler show an excess loss of only 0.1dB and an imbalance of less than 0.02dB for both TE and TM



(a)



(b)

**Figure 1:** (a) Rib waveguide cross sectional view and (b) MMI top view.

polarizations. In the  $1.5\mu\text{m}$  to  $1.6\mu\text{m}$  bandwidth they remain lower than 0.6dB and 0.05dB, respectively. In section 2 we briefly review some basic MMI theory, which is further discussed for rib waveguides in section 3. From the spectral analysis of the fundamental mode of the rib access waveguides we derive, in section 4, a design criterion for these waveguides, which is applied to two  $2 \times 2$  MMIs in section 5.

## 2 Idealized MMI imaging

Fig. 1(b) shows a schematic top view of a  $2 \times 2$  MMI coupler. The access wave-guides are numbered from 1 to 4, and have a width of  $W_W$ , while the multi-mode (or imaging) region is  $L_{MMI}$  long and  $W_{MMI}$  wide. Light coming into the device through one of the waveguides excites several modes inside the multimode region which, after a certain distance, interfere to form self-images of the excitation. By placing the output waveguides in the position of these images the input power is divided between the output waveguides.

In the following we briefly review the basic MMI model established in [1], on which our further discussion will be based.

Under a 2D approximation, that is, ignoring the  $y$  dimension, the electromagnetic field of the access waveguide,  $f(x)$ , is completely expanded into the modes of the multimode section, i.e.,  $f(x) = \sum_m c_m \varphi_m(x)$ , where  $\varphi_m(x)$  may be approximated as

$$\varphi_m(x) = \sin\left(\frac{m\pi}{W_{MMI}}x\right), \quad m = 1, 2, 3, \dots \quad (1)$$

The imaging then takes place at certain propagation

distances because the propagation constants  $\beta_m$  of the  $\varphi_m(x)$  modes are related by a parabolic law, namely  $\beta_m = \beta_1 - (m^2 - 1) \times const$ . If this relationship is not fulfilled no perfect imaging is possible.

The excitation coefficients  $c_m$  are calculated by means of the overlap integral

$$c_m = \frac{2}{W_{MMI}} \int_0^{W_{MMI}} f(x) \sin\left(\frac{m\pi}{W_{MMI}}x\right) dx \quad (2)$$

Please note that, according to this definition,  $c_m$  are also the Fourier coefficients of  $f(x)$ .

### 3 MMI imaging in rib waveguides

In this section we will study to which extent the conditions for perfect imaging can be met in rib waveguides. In order to do so, we will study into which kind of modes of the multimode section the input field of the access waveguides can be expanded. We shall only consider imaging in the  $x$  direction, which is desired in most practical devices, as opposed to 3D imaging that also takes place in the  $y$  direction [9]. In the following we will use  $TX_{m,n}$  to refer to rib waveguide modes with  $m$  half cycles in the lateral direction and  $n$  half-cycles in the vertical direction of both TE and TM polarizations. Let us consider the two TE modes of a rib multimode section shown in fig. 2(a) and 2(b).

In a 2D approximation where the height of the device is “compressed” to zero, the  $TE_{41}$  mode in fig. 2(a) would be well approximated by a sine function like  $\varphi_4(x)$  (see eq. 1). Obviously, the same is true for all  $TX_{m,1}$  modes, which means that their propagation constants will follow the parabolic law required for imaging. Thus, we will call such modes “imaging modes”, because if only these modes were excited we would be in the same situation as in the 2D case (section 2), and imaging would be virtually perfect.

On the contrary, the  $TE_{12}$  mode in fig. 2(b) is a “non-imaging mode”, because due to its two half-cycles in the  $y$  direction, its propagation constant cannot fit the parabolic law of the imaging modes. Consequently, if this mode were excited, it would propagate through the multi-mode region along with the imaging modes, but it would not properly contribute to image formation, thus deteriorating the image quality and the device’s performance. Generally, any  $TX_{m,n}$  mode with  $n \geq 2$  is a non-imaging mode.<sup>1</sup>

In conclusion, for imaging to work properly, we have to make sure that all the power of the input excitation is coupled into imaging modes, that is, guided modes with one half-cycle in the vertical direction. How the power of the input is distributed into the different modes of the imaging region depends on the shape of the input field, which will be analyzed in the next section.

### 4 Input mode field spectrum

We will now derive a criterion for the input waveguide dimensions which ensures that only imaging modes are

excited in the multimode region. The input excitation is supposed to be the fundamental mode of the access waveguide. Fig. 2(c) shows the fundamental TE mode of single-mode rib waveguide (its dimensions fulfill Soref’s condition [4]).

In order to find out what kind of modes this field excites inside the imaging region one option is to solve the discontinuity between the access waveguide and the imaging section. This can be done for example with a software like Fimmprop<sup>2</sup>, but while this yields the rigorous result, it gives little insight into the problem. This is why we also use a second approach, based on an idealized (rectangular) imaging section of width  $W_{MMI}$  and height  $H$  that supports an infinite number of sine like modes

$$\varphi_{m,n}(x, y) = \sin\left(\frac{m\pi}{W_{MMI}}x\right) \sin\left(\frac{n\pi}{H}y\right), \quad m, n = 1, 2, 3, \dots \quad (3)$$

whose excitation coefficients are given by

$$c_{m,n} = \frac{4}{HW_{MMI}} \int_0^{W_{MMI}} \int_0^H E_d(x, y) \varphi_{m,n}(x, y) dx dy \quad (4)$$

where  $E_d$  is the dominant field component of the mode, that is  $E_x$  for TE polarization and  $E_y$  for TM polarization. Note that eq. (3) and (4) are simply extension of eq. (1) and (2) and that  $\varphi_{m,1}$  are the imaging modes. Since the  $c_{m,n}$  coefficients can be interpreted as the (bidimensional) Fourier coefficients of  $E_d$ , the quantities

$$p_n = \frac{\sum_m |c_{m,n}|^2}{\sum_m \sum_n |c_{m,n}|^2} \times 100\% \quad (5)$$

are the fraction of power of the input field that, in an idealized imaging region, would couple into all modes that have  $n$  half-cycles in the vertical direction. Particularly, the fraction of power that would couple into the imaging modes  $\varphi_{m,1}$  is given by  $p_1$ .

If we analyze the mode of a typical single mode rib waveguide as the one in fig. 2(c) we get  $p_1 = 93\%$ ,  $p_2 = 6.6\%$ ,  $p_3 = 0.1\%$ . That means that even in an idealized imaging section only 93% of the power would couple into imaging modes so that a power loss of at least  $-10 \log_{10}(0.93) \approx 0.3\text{dB}$  is to be expected. It is also very interesting to note that nearly all the remaining power couples into  $\varphi_{m,2}$  modes, that is, modes of the same type as the one shown in fig. 2(b). This fact can be exploited to estimate more easily the fraction of power that couples into imaging modes. All the  $\varphi_{m,n}$  modes with  $n$  odd are symmetrical with respect to  $y = \frac{H}{2}$ , whereas the modes with  $n$  even are anti-symmetrical. Since virtually all the power that couples into symmetric modes couples into the imaging modes ( $p_1 \gg p_3$ ), their power may be estimated as the power in the symmetric part of the input field:

$$P_{symm} = \frac{\iint_{\Omega} |E_d(x, y) + E_d(x, H - y)|^2 dx dy}{4 \iint_{\Omega} |E_d(x, y)|^2 dx dy} \times 100\% \quad (6)$$

<sup>1</sup>This is only true when no 3D imaging is considered.

<sup>2</sup>Fimmprop is an eigenmode expansion based tool and is part of the Fimmwave package by Photon Design: [www.photon.d.com](http://www.photon.d.com)

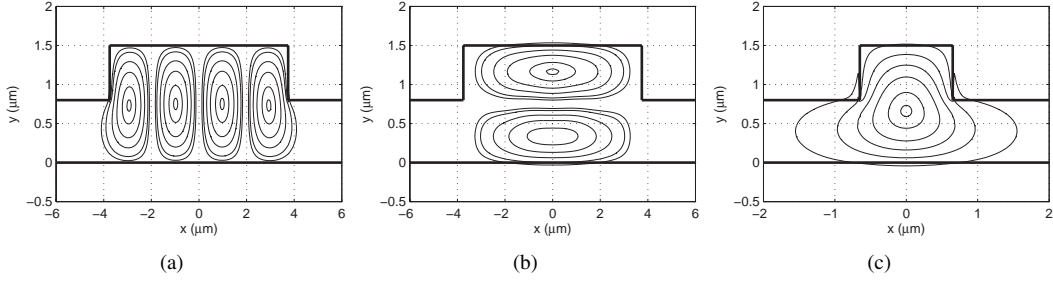


**Figure 2:** (a) and (b): Two modes of a shallowly etched multimode section ( $W_{MMI} = 7.5\mu\text{m}$ ) (a) Example of an imaging mode ( $\text{TE}_{41}$ ) (b) Example of a non-imaging mode ( $\text{TE}_{12}$ ). (c):  $\text{TE}_{11}$  mode of a single mode access waveguide ( $W_W = 1.3\mu\text{m}$ ); In all three figures  $H = 1.5\mu\text{m}$ ,  $D = 0.7\mu\text{m}$ .

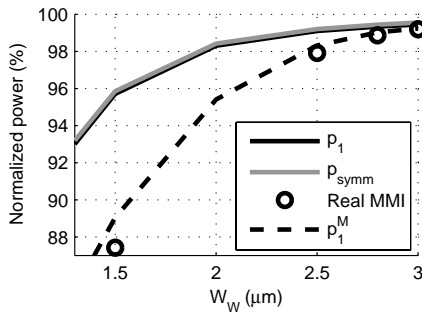


**Figure 3:** Fraction of power coupled from the  $\text{TE}_{11}$  mode of a rib waveguide into the imaging modes of a  $W_{MMI} = 7.5\mu\text{m}$  wide multimode section as a function of  $W_W$  ( $H = 1.5\mu\text{m}$ ,  $D = 0.7\mu\text{m}$ ).

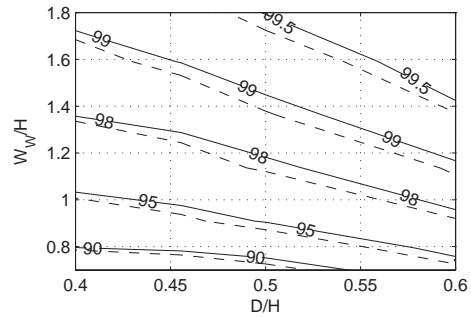


**Figure 4:** Symmetry factor  $p_{symm}$  [eq. (6)] as a function of the rib aspect ratios  $W_W/H$  and  $D/H$  (solid lines:  $H = 1.5\mu\text{m}$ , dashed lines:  $H = 2.2\mu\text{m}$ ).

where  $\Omega$  is the waveguide's cross-section. This result is actually rather intuitive: since all the imaging modes are symmetric with respect to  $y = \frac{H}{2}$ , their superposition can only represent excitations with the same kind of symmetry. Fig. 3 illustrates how the fundamental mode of a shallowly etched rib waveguide becomes more symmetrical as the waveguide width ( $W_W$ ) is increased, so that more power couples into the imaging modes of the idealized multimode section (curves  $p_{symm}$  and  $p_1$ ). The data labeled "Real MMI" in fig. 3 represents the fraction of power coupled into the imaging modes of the real (rib) multimode section as simulated with Fimmprop. For small widths the real coupling is lower than predicted by the idealized model, but this is simply because the number of imaging modes supported by the rib structure is limited, so that its resolution is too low to completely represent the symmetric part of the input field. Actually, if we convert the rib multimode section into a slab waveguide using the effective index method, calculate the number of modes ( $M$ ) it supports, and define  $p_1^M = \frac{\sum_{m=1}^M |c_{m,n}|^2}{\sum_m \sum_n |c_{m,n}|^2} \times 100\%$ , we obtain a much better agreement between the model and the simulated data (curve  $p_1^M$  in fig. 3). Anyhow, by the time the input fields becomes highly symmetric ( $p_{symm} \geq 98\%$ ), it is also wide enough to be faithfully

represented by the real imaging modes.

The conclusion of this section and one of the main points of this communication is thus that for imaging to work properly, the input waveguides have to be designed so that their fundamental TE and TM modes are highly symmetric in the vertical direction ( $p_{symm} \rightarrow 100\%$ ) [eq. (6)].

## 5 Design

At this point we are ready to design two MMIs based on the criterion established in the previous section. We start by calculating the symmetry factor  $p_{symm}$  for a set of common rib aspect ratios and for two different substrate heights. From the results shown in fig. 4 it is clear that the symmetry is higher for wider waveguides (as already observed in fig. 3), but also for deeply etched waveguides, which explains the good performance of deeply etched MMIs. It is also noticeable that  $p_{symm}$  only weakly depends on the absolute substrate height  $H$ , so that the chart is probably also useful for other values of  $H$ . It has to be pointed out that the results are given only for the TE polarization, as we have found that the TM modes always have a slightly higher symmetry factor (probably because their confinement is better), so that the TE polarization is actually the worst case.

For our design we chose a substrate height of  $H =$

**Table 1:** Dimensions of the optimized general and paired interference based MMIs (all values are in  $\mu\text{m}$ ).

	$W_{MMI}$	$L_{MMI}$	$W_W$	$s$
General	7.5	274	2.8	1.5
Paired	12.8	256	2.8	1.5

$1.5\mu\text{m}$  and an etching depth of  $D = 0.7\mu\text{m}$ , so that a waveguide with  $W_W < 1.4\mu\text{m}$  is single-moded [4]. While such a single mode waveguide is useful as in interconnecting waveguide within a larger circuit [10], it is not adequate as MMI access waveguide, because its fundamental mode has a low symmetry factor. Actually, according to fig. 4, since  $D/H \approx 0.46$ , to achieve  $p_{symm} \geq 99\%$  one has to choose  $W_W \geq 1.6 \times 1.5 \approx 2.4$ . In order to make the design somewhat tolerant to etching depth fluctuations, we set  $W_W = 2.8\mu\text{m}$ , so that the required symmetry is maintained even if the etching depth were only  $D = 0.6\mu\text{m}$ . Obviously this requires an adiabatic taper between the interconnecting single mode waveguide and the MMI access waveguide; we intend to address this issue in the near future.

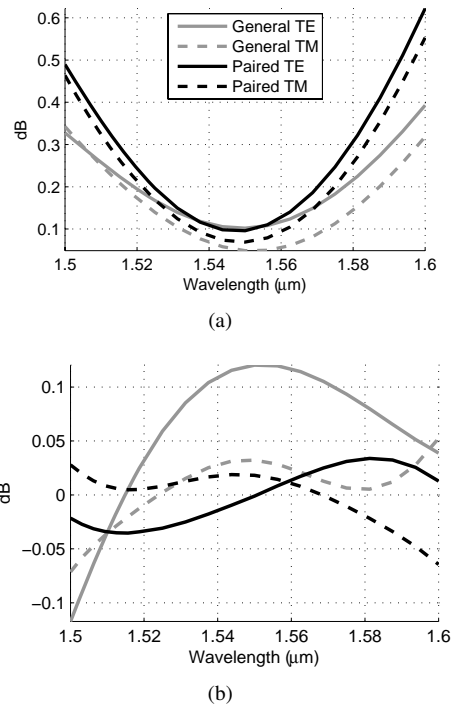
The next step in the design of the MMI is to determine the minimum separation between the access waveguides to avoid coupling between them. Using Fimmprop, we found that a separation of  $s = 1.5\mu\text{m}$  (see fig. 1(b)) yields satisfactory values.

We designed two  $2 \times 2$  couplers, one based on general interference and another one based on paired interference [2], whose minimum widths are given by  $W_{MMI}^G = 2W_W + s = 7.1\mu\text{m}$  and  $W_{MMI}^P = 3(W_W + s) = 12.9\mu\text{m}$ . To numerically optimize the width and length of the devices, we have used the fact that length scans are very fast in Fimmprop so that the following procedure could be used:

1. For the initial width, find the optimum length of the device, in the sense of a tradeoff between minimum excess loss and minimum imbalance.
2. Decrease the width by  $0.1\mu\text{m}$  and find the optimum length of the device. If the tradeoff between excess losses and imbalance is improved, repeat this step until no further improvement is achieved. If the performance is worse, increase the width.

Excess loss and imbalance are defined as usual,  $EL = -10 \log_{10} \left( \frac{P_3 + P_4}{P_1} \right)$  and  $IB = -10 \log_{10} \left( \frac{P_3}{P_4} \right)$ , where  $P_i$  denotes the power of the fundamental mode in access waveguide  $i$  (see fig. 1(b)), and the excitation was launched from waveguide 1.

The final dimensions of the devices are given in table 1 and their performance is shown in fig. 5. While both devices exhibit very low excess losses and imbalance for both polarizations, it can be seen that the general interference based MMI has slightly lower excess loss in the extremes of the bandwidth, whereas the paired interference based device offers a better imbalance.

**Figure 5:** (a) Excess losses and (b) imbalance of the designed MMIs as a function of wavelength.

## Conclusion

We have presented a design procedure for single etch step, high performance MMIs based on the symmetry factor of their access waveguides [eq. (6)]. Two devices with potentially single mode access waveguides have been designed, and optimized via simulations, yielding very promising values of excess loss and imbalance, which can easily compete with those reported for the two etch step design in [7].

## Acknowledgments

This work was supported by the Spanish Ministerio de Educación y Ciencia under project TEC2006-02868.

## References

- [1] M. Bachmann et al, Applied Optics, no. 33, p. 3905, 1994
- [2] L.B Soldano et al, J. Lightwave Tech., no. 13, p. 615, 1995
- [3] B. Jalali et al, Sel. Topics Quantum Electronics, no. 4, p. 938, 1998
- [4] R.A. Soref et al, J. Quantum Electronics, no. 27, p. 1971, 1991
- [5] J. Lousteau et al., J. Lightwave Tech., no. 22, p. 1923, 2004
- [6] H. Wei et al, Optics Letters, no. 12, p. 878, 2001
- [7] D. Dai et al, Applied Optics, no. 24, p. 5036, 2005
- [8] Y. Tang et al, Optical Engineering, no. 43, p. 2495, 2004
- [9] M. Rajarajan et al, J. Lightwave Tech., no. 9, p. 2078, 1996
- [10] R. Halir et al, J. Optical & Quantum Elec., to be published